Progress In Electromagnetics Research Letters, Vol. 111, 27–34, 2023

Novel Passive Intermodulation Measurement Platform for Planar Microwave Circuit

Junqiang Yang[1], Xiong Chen[1, *], and Qianwen Chen[2, *]

Abstract—This paper presents a novel test platform for passive intermodulation measurement on planar microwave circuits using a filter design strategy. A finger planar band-pass filter is proposed and optimized to have an evenly distributed stimulation field on the surface. The layout is optimized with symmetrical coupling lines from two directions, and the feed line is with a tapered transformer. A pair of T-type resonators is adopted to improve the flatness of the field distribution. In the application of this test platform, print circuit boards with different layouts are tested, and the passive intermodulation difference of different layouts can be differentiated. As this platform is an open space, the device under test can be easily replaced without suspending the passive intermodulation test system, which can be applied in the production line to speed up the production quality inspection.

1. INTRODUCTION

Passive intermodulation (PIM) is a phenomenon of nonlinear distortion caused by the electromagnetic nonlinearity of passive components. This distortion originates from either non-ideal metal contact or the use of a nonlinear material [1, 2]. PIM can generate interference signals that seriously degrade the performance of communication systems, especially in high-power applications. When the PIM product resulting from the mixing of two or more RF carriers falls into the sensitive receiving frequency band, it can cause significant interference to the receiver [3–6].

For all kinds of transmission lines in microwave applications, printed circuit boards (PCBs) play an indispensable role in the communication equipment. PCBs are widely used in high-power multi-channel transmitters, sensitive receivers, and shared antennas due to their ability to construct various microwave functions. The electromagnetic compatibility problem in high-density microwave devices makes these applications sensitive to PIM distortion [7]. In most high-power applications, PCBs are the most commonly used components and are therefore at a higher risk of being affected by PIM distortion due to their widespread use. The early method to measure PIM characterization on PCBs is by measuring the forward and reverse PIM products between the input and output ports of microstrip lines fed by carriers [2]. However, the PIM performance of a PCB specimen is characterized by the total PIM response of multiple distributed nonlinear sources, and it is difficult to locate the source of the nonlinearity. Traditional PIM tests require the suspension of the PIM system and the disconnection and reconnection of the test loop, which can introduce additional test uncertainties. Although near-field probing has been shown to be a powerful experimental tool for mapping PIM product distributions in PCBs [7], its small sensitive area necessitates a redundant sweeping operation around the device under test (DUT) surface, which can result in additional human cost, especially for DUTs with large areas. To quickly locate the PIM source and check the PIM product in a large PCB, a test platform with a remarkable scanning surface is needed.

Received 19 February 2023, Accepted 15 May 2023, Scheduled 19 June 2023
* Corresponding authors: Xiong Chen (shawn.cc@foxmail.com), Qianwen Chen (chenqianwen12358@126.com).
[1] School of Microelectronics, Tianjin University, Tianjin 300072, China. [2] Hunan University, China.

In this paper, we propose a new planar test setup for near field probing of PIM products in PCBs. While different PCB layouts are measured, their different PIM components are compared. This work is structured as follows. The design of this platform is provided in Section 2, while the measurement and discussion are provided in Section 3.

2. PIM TEST PLATFORM DESIGN

For the fast production line test requirement, an on-line PIM test flow is proposed as shown in Fig. 1. The platform with the PIM test loop serves as a continuous setup for testing different DUTs. The addition of DUTs does not significantly change the voltage standing wave ratio (VSWR) of this test loop, so PIM measurements are not interrupted, and there is no need to disconnect and reconnect cables, which accelerates the testing process and reduces uncertainties caused by repeated connection operations. The design of the test platform refers to the design of the planar filter using microstrip, and the coupling field on the filter surface is optimized to be evenly distributed on the planar filter surface. The strong near-field coupling between the band-pass filter and the PCB under test is used to detect the PIM products.

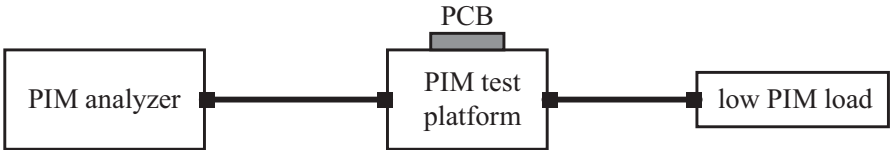

Figure 1. Schematic diagram of PIM on-line test.

The designed layout is shown in Fig. 2(a), consisting of 50 Ω transmission lines, tapered transformers, interdigital coupled lines, and T-type resonators. For this layout, the core components are two T-type resonators, and this pair of open-step loaded resonators is used to regulate and control the bandwidth and resonant frequency. Fig. 2(b) shows the typical schematic of an open-stub loaded resonator, which consists of a half-wave length resonator and an open circuit of transmission line, where Z_1, l_1, Z_2, and l_2 denote the characteristic impedances and lengths of the microstrip line and open-stub, respectively. An odd- and even-mode will be used to analyze the proposed dual-mode structure due to the symmetrical structure of the circuit. The circuit structure of Fig. 2(b) can be divided into an odd- and even-mode as shown in Fig. 2(c) and Fig. 2(d), respectively [8].

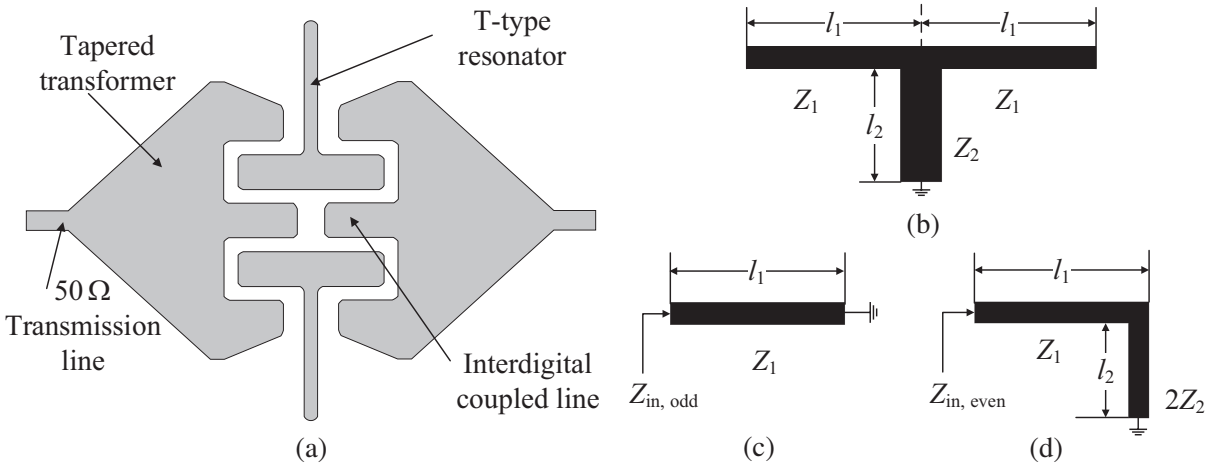

Figure 2. (a) The designed layout of test platform. (b) Schematic of the T-type resonator using open-stub loaded. (c) Equivalent circuit of odd-mode resonance. (d) Equivalent circuit of even-mode resonance.

The odd-mode is identical to that of the single-mode half-wave length resonator. This leads to the approximate equivalent circuit of Fig. 2(c). Under the odd-mode resonance condition of $Z_{in,odd} = \infty$, the fundamental odd-mode (f_{odd}) resonant frequency can be expressed as

$$f_{odd} = \frac{c}{4l_1\sqrt{\varepsilon_e}} \tag{1}$$

For even-mode excitation, the approximate equivalent circuit is shown in Fig. 2(d). From the even-mode resonance condition of $Z_{in,even} = \infty$ and suppose $Z_1 = 2Z_2$, the fundamental even-mode resonant frequency (f_{even}) can be expresses as

$$f_{even} = \frac{c}{2(l_1 + l_2)\sqrt{\varepsilon_e}} \tag{2}$$

From (1) and (2), it is easy to conclude that the odd mode resonant frequency depends only on the length of the resonator l_1, which has no relation with the length of the open-step loaded l_2. In contrast, the even mode resonant frequency is related to l_1 and l_2 [9]. Hence, the open-stub load has not affected responses at an odd-mode resonant frequency, wherein the even-mode resonant frequency can be flexibly changed. By tuning these pairs of geometry parameters, the designed center frequency can be determined [10].

The equivalent circuit model of Fig. 2(a) is shown in Fig. 3. In this circuit model, L_1 represents the inductance caused by the 50 Ω transmission line, and the tapered transformer is considered as inductance L_2. Due to the different thicknesses of the substrate on the two sides, the impedance exhibits a step, which is expressed by capacitance C_1. The inter-digital coupled lines are modeled by L_4, C_2, and L_5, C_5. The parameter C_3 represents the capacitive coupling between the inter-digital coupled lines and the T-type resonator. Parameters L_3 and L_4 represent the inductance caused by the T-type resonator. At the open end of the open-stub, the fields do not stop abruptly but extend slightly further due to the fringing field, which is modeled by an equivalent shunt capacitor C_4. Resistor R_1 represents the parasitic resistance of inductor L_5, and R_2 is the ground resistance of inductor L_3. Finally, the Advanced Design System (ADS) circuit simulator is used to solve and simulate the model.

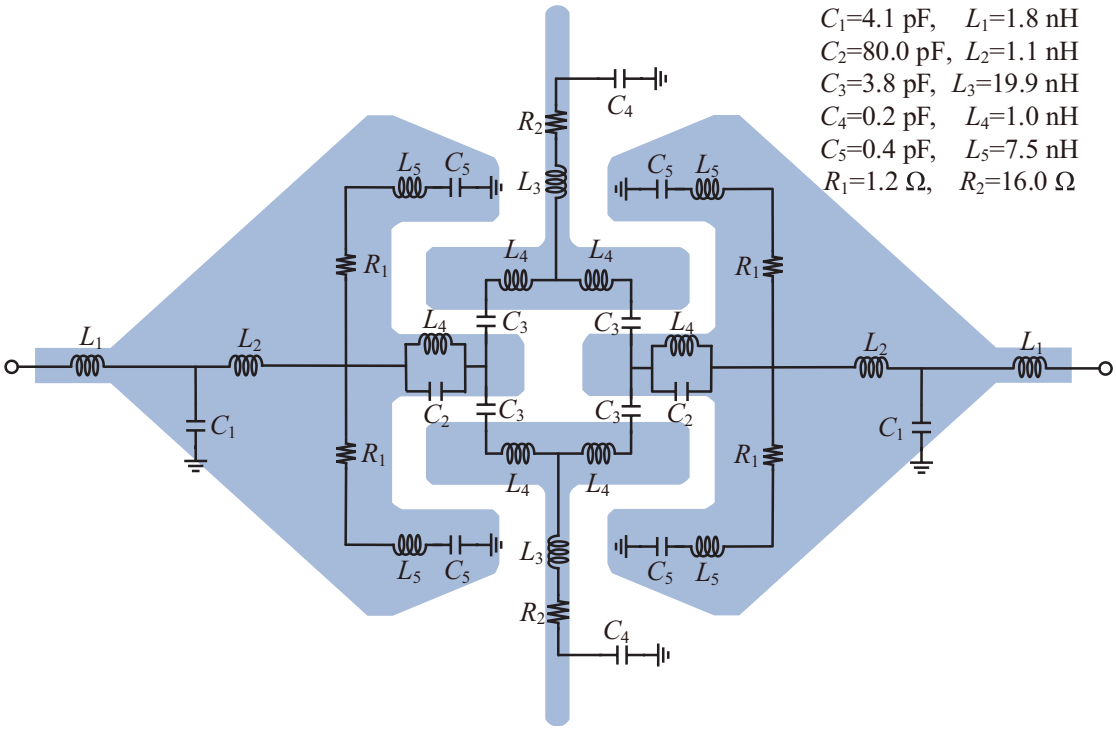

Figure 3. Equivalent circuit model of test platform.

As shown in Fig. 4, the proposed test platform is implemented on the polytetrafluoroethylene (PTFE) substrate with a thickness of 11 mm and permittivity of 2.04. The final optimized dimensions of the T-type resonators and the inter-digital coupled lines have been obtained by using finite element simulation. Their electrical performances are then simulated.

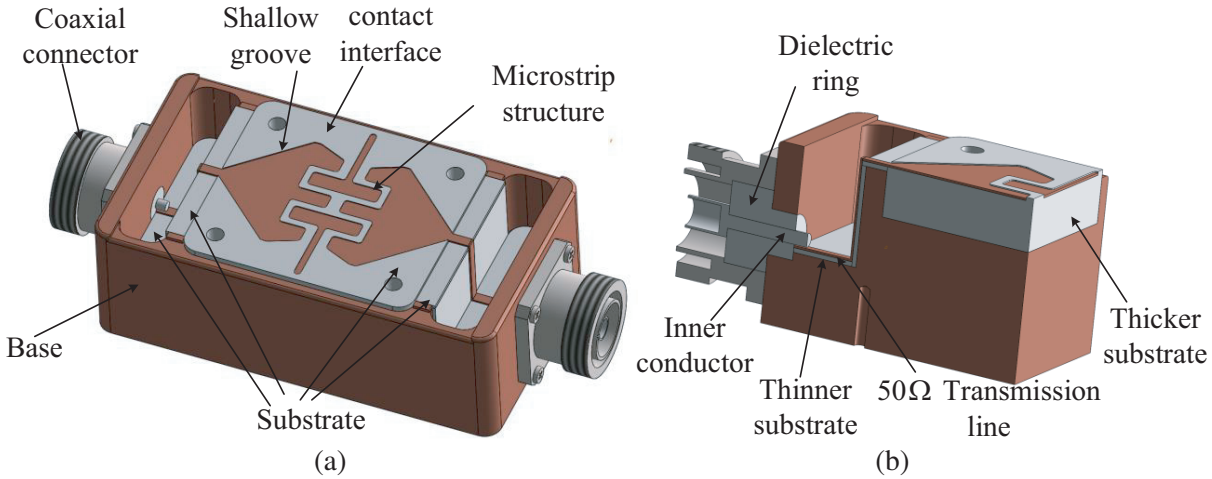

Figure 4. (a) The test platform. (b) Section view of PIM test platform.

The PIM test platform with coaxial connector is shown in Fig. 4(a), and its main structure can be equivalent to a microstrip band-pass filter. A shallow groove with a corresponding shape is provided on a thicker substrate, and a corresponding microstrip line is placed in the shallow groove. As shown in Fig. 4(b), the inner conductor of a low PIM coaxial connector is soldered together with a 50 Ω transmission line on a thinner substrate to complete the connection. As the microstrip line structure is placed in the shallow groove, the PCB under test can be placed directly on it without contacting the microstrip line structure. As the surface of the whole device is flat, the PIM test can continue even in PCB moving operations, significantly improving test efficiency. After manufacturing, the measurements of the test platform are compared with the equivalent circuit and electromagnetic simulation, and the results are relatively consistent as shown in Fig. 5, while the simulated field distribution is shown in

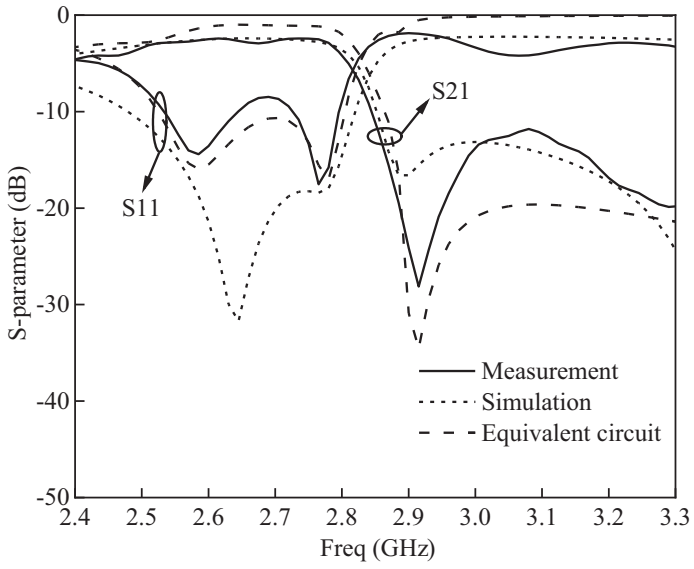

Figure 5. *S*-parameters of test platform from measurement, simulation, and equivalent circuit.

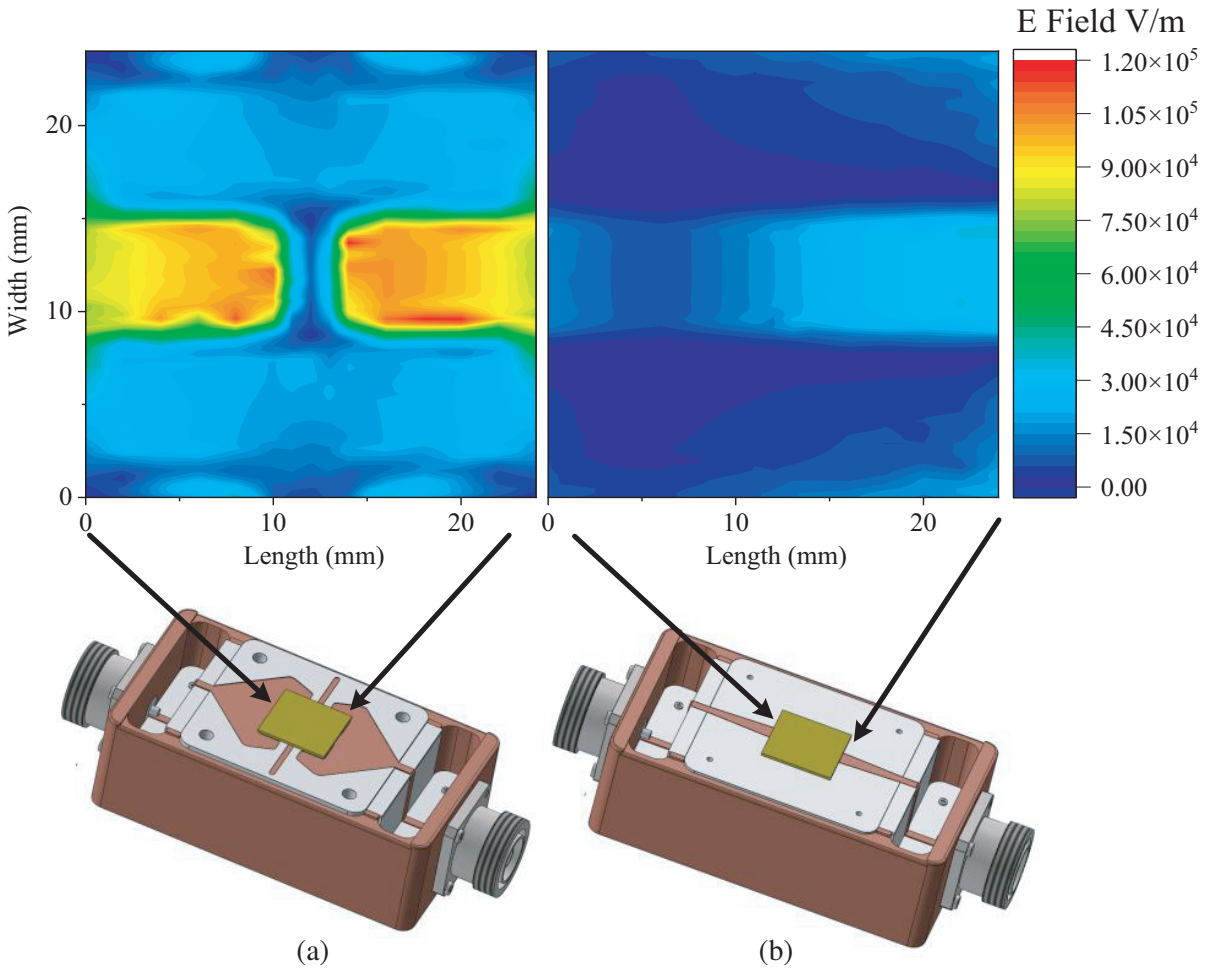

Figure 6. The electric field distribution (a) on the surface of the platform, (b) on a micro-strip transmission line.

Fig. 6 (a single-sided copper-plated FR-4 board is placed on the platform).

Figure 6(a) shows the electric field distribution mapped on the surface of the platform at the PIM frequency under test (2.564 GHz). Under the same conditions, the electric field distribution at the same distance on the surface of the microstrip transmission line is shown in Fig. 6(b). Compared with the electric field on the interdigital platform shown in Fig. 6(a), it radiates a limited electric field intensity and is concentrated on the trajectory of the microstrip line. The comparison of Fig. 6(a) and Fig. 6(b) shows that the design optimizes the field distribution, making the field not only stronger, but also more uniform. The optimized field distribution improves the PIM response on the DUT, resulting in better test results.

3. MEASUREMENT AND DISCUSSION

The measurement is based on PIM analyzer, and the carriers are at 2.620 GHz and 2.676 GHz with equal power of 43 dBm, while the PIM frequency is at 2.564 GHz. The test PCB sample is placed horizontally on the middle surface of the test platform. In this demonstration, the PIM difference from different layouts is the study object. In order to minimize the potential PIM risk generated from the copper ground or PCB laminate properties, the PCB sample without wiring is taken as a reference. The stable residual PIM level of the reference is below -125 dBm @2×43 dBm. Fig. 7 shows a photograph of the PCB samples and the PIM test platform, and the impedance of microstrip lines is 50 Ω.

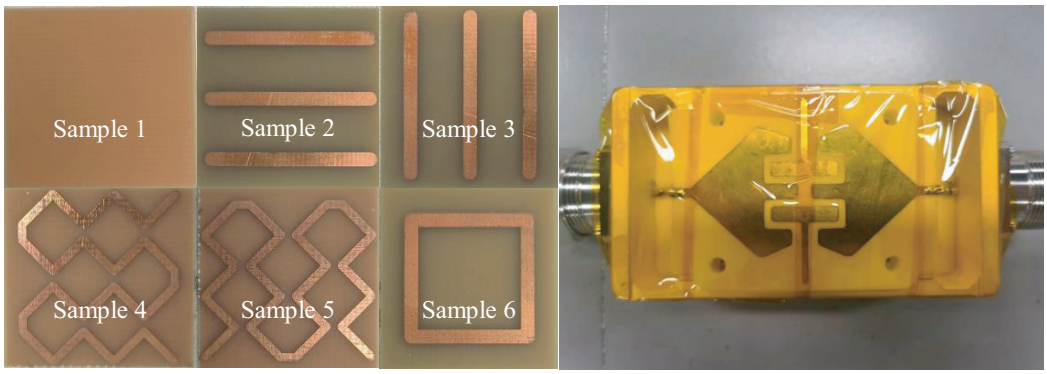

Figure 7. The photograph of the PCB samples and the PIM test platform.

The measurement results of the PCB samples are shown in Fig. 8. The electric field component E_z perpendicular to the sample surface is the simulation result of single-carrier excitation at the PIM frequency. It can be observed that the device can identify the PIM level of different samples. Sample 1 represents a PCB without wiring, and its PIM value is slightly higher than the residual PIM. It can be seen that the characteristics of PCB laminates have a small contribution to PIM. The test results of samples 2, 3, 4, 5, and 6 show that the wiring on the PCB has a large impact on the PIM level. Samples 3 and 5 are obtained by rotating samples 2 and 4 by 90 degrees, respectively. The PIM level of samples 2 and 4 is much higher than that of samples 3 and 5 because the lines on samples 2 and 4 follow the wave propagation direction, and the electric field intensity obtained by coupling is higher. The lines on samples 4 and 6 are discontinuous, which is easier to produce intermodulation than that on sample 2, so the test results of PIM3 values in Figure 8(a) is higher. The electric field intensity obtained by coupling on sample 6 is the highest, so the PIM level is the highest. As shown in Fig. 8(a), the electric field intensity obtained by near-field coupling on the simulated PCB sample is consistent with the trend of the tested PIM level. The simulated electric field intensity and the tested PIM level of sample 6 at different positions (as shown in Fig. 9, from a to h and their symmetrical positions a' to h') of the platform are shown in Fig. 8(b), which shows the same trend and can prove the effectiveness of the test.

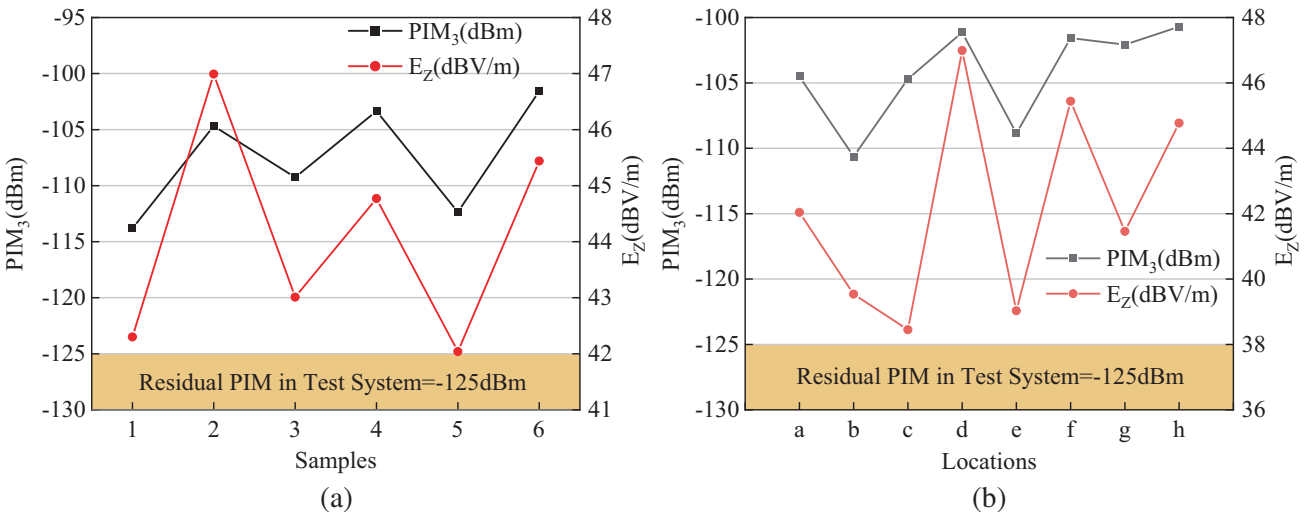

Figure 8. The simulated E_z distribution at the carrier frequency in the case of single-carrier excitation comparison with the measurement results of (a) PCB samples and (b) sample 6 at different positions (from a to h) of the platform.

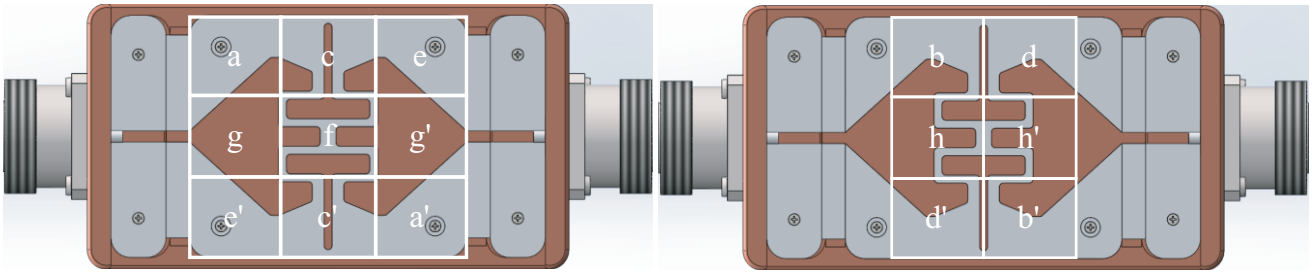

Figure 9. The position (from a to h and their symmetrical positions a' to h') of PCB samples placed on the platform.

4. CONCLUSION

A test platform based on planar field coupling to measure the PIM level of PCBs with different layouts is demonstrated. The PIM products of several PCB samples with different layouts are measured and compared, and the distinct PIM product differences of different PCB samples prove the effectiveness of the proposed test platform. The experimental results show that the geometry of microstrip lines on the PCB will affect PIM levels. The research provides a practical solution for quick PIM testing on PCB of industrial pipeline. With the proposed test platform, an on-line PIM test system can be built. This set of test system does not require any suspension of the PIM test system in the measurement and replacement of DUT, which can be applied on the production line to realize quick production quality inspection.

ACKNOWLEDGMENT

This work was supported in part by the National Natural Science Foundation of China under Grant of 62271240, and in part by the National Key Laboratory Foundation 2021-JCJQ-LB-006 (Grant No. 6142411122115).

REFERENCES

1. Hienonen, S., V. Golikov, P. Vainikainen, and A. V. Raisanen, "Near-field scanner for the detection of passive intermodulation sources in base station antennas," *IEEE Transactions on Electromagnetic Compatibility*, Vol. 46, No. 4, 661–667, Nov. 2004.
2. Shitvov, A. P., D. E. Zelenchuk, A. G. Schuchinsky, and V. F. Fusco, "Passive intermodulation generation on printed lines: Near-field probing and observations," *IEEE Transactions on Microwave Theory and Techniques*, Vol. 56, No. 12, 3121–3128, Dec. 2008.
3. Chen, X., Y. He, S. Yang, et al., "Analytic passive intermodulation behavior on the coaxial connector using monte carlo approximation," *IEEE Transactions on Electromagnetic Compatibility*, Vol. 60, No. 5, 1207–1214, Oct. 2018.
4. Hienonen, S., V. Golikov, V. S. Mottonen, P. Vainikainen, and A. V. Raisanen, "Near-field amplitude measurement of passive intermodulation in antennas," *2001 31st European Microwave Conference*, 1–4, London, UK, 2001.
5. Zhang, W. and F. Nian, "The construction and analysis of PIM testing system," *2012 International Conference on Microwave and Millimeter Wave Technology (ICMMT)*, 1–4, Shenzhen, 2012.
6. Yong, S., S. Yang, L. Zhang, X. Chen, D. J. Pommerenke, and V. Khilkevich, "Passive intermodulation source localization based on emission source microscopy," *IEEE Transactions on Electromagnetic Compatibility*, Vol. 62, No. 1, 266–271, Feb. 2020.

7. Shitvov, A. P., D. D. Zelenchuk, A. G. Schuchinsky, V. F. Fusco, and N. Buchanan, "Mapping of passive intermodulation products on microstrip lines," *2008 IEEE MTT-S International Microwave Symposium Digest*, 1573–1576, Atlanta, GA, USA, 2008.
8. Song, K. and Q. Xue, "Novel broadband bandpass filters using Y-shaped dual-mode microstrip resonators," *IEEE Microwave and Wireless Components Letters*, Vol. 19, No. 9, 548–550, Sept. 2009.
9. Tantiviwat, S., M. S. Razalli, and S. Z. Ibrahim, "Miniature microstrip bandpass filters based on quadruple-mode resonators with less via," *2017 IEEE MTT-S International Conference on Microwaves for Intelligent Mobility (ICMIM)*, 1–4, Nagoya, 2017.
10. Sun, S. and L. Zhu, "Capacitive-ended interdigital coupled lines for UWB bandpass filters with improved out-of-band performances," *IEEE Microwave and Wireless Components Letters*, Vol. 16, No. 8, 440–442, Aug. 2006.